Nanoscale Advances

REVIEW

View Article Online
View Journal | View Issue

Cite this: *Nanoscale Adv.*, 2021, **3**, 2411

Tailoring silver nanoclusters *via* doping: advances and opportunities

Jie Yang, *[a] Runqiang Pang,[a] Dongpo Song [a] and Man-Bo Li *[bc]

Atomically precise noble metal nanoclusters (especially Au and Ag) have been pursued due to their fascinating molecule-like properties. In spite of the significant progress on Au nanoclusters (NCs), the structure and property evolution of Ag NCs is still in high demand. Doping is a useful strategy for improving the physicochemical performances of Ag NCs. Herein we summarize the recent advances in tailoring silver NC structures and properties *via* doping. First, we reviewed the recent studies on the synthesis of hetero metal atom doped silver bimetallic nanoclusters, which are classified by the dopants, including Au, Pt, Pd, Cu, Ni and Cd. Second, the doping effects on their properties were reviewed, including the locations of hetero metal atoms, the influence on their stability, and the charge state evolution. Moreover, we highlighted the doping-dependent improvement of the photo-luminescence (PL) performance and catalytic activity of Ag NCs.

Received 30th January 2021
Accepted 8th March 2021

DOI: 10.1039/d1na00077b

rsc.li/nanoscale-advances

1. Introduction

Atomically precise metal nanoclusters (NCs) composed of a discrete number of metal atoms and monodisperse coordination ligands have raised immense scientific interest. They are unique materials, which are stable at a smaller scale (<2 nm) compared with nanoparticles and still retain molecule-like characteristics, such as luminescence, molecular magnetism, chirality, *etc.*[1–6] Furthermore, their identified formulas and atomically precise structures provide atomic-level structure–property correlation and modification.

As the two most outstanding species, gold and silver NCs showed different performances in stability. Improving the stability and enhancing their diverse properties is the major priority in studying Ag NCs. Adding hetero-metal atoms into the mono-metal kernel has been demonstrated to be an effective strategy to obtain stable and functional Ag NCs, where doping methods have been extensively carried out to tailor Ag NC properties in recent studies. Generally, doping with foreign atoms will tune the geometric and electronic structures of NCs and further influence their optical properties and catalytic activity. Moreover, doping endows Ag NCs with better thermal stability.[7–12]

[a]*School of Materials Science and Engineering, Jiangsu University of Science and Technology, Zhenjiang 212003, China. E-mail: yjolah@just.edu.cn*
[b]*Institute of Physical Science and Information Technology, Anhui University, Hefei, Anhui, 230601, P. R. China. E-mail: mbli@ahu.edu.cn*
[c]*Hefei National Laboratory for Physical Sciences at the Microscale, Hefei, Anhui, 230026, P. R. China*

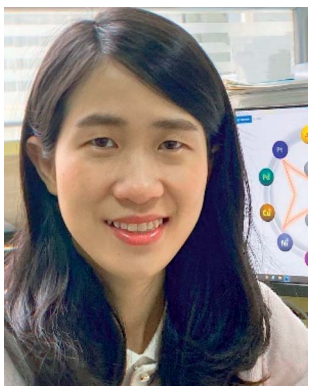

Jie Yang is currently an Associate Professor of Materials Science and Engineering at Jiangsu University of Science and Technology. She received her PhD degree in MSE from the University of Science and Technology of China in 2015. Then she joined the MSE faculty of JUST in 2016, and she worked at Carnegie Mellon University (CMU, Pittsburgh, USA) in 2019. Her research interests include the synthesis of atomically precise metal nanoparticles and their alloys.

Runqiang Pang is currently a master's candidate in Materials Science and Engineering under the supervision of Prof. Jie Yang in Jiangsu University of Science and Technology. Her research interests focus on the syntheses and properties of silver nanoclusters and their alloy nanoclusters.

To understand the fundamental mechanism for the rational design of functional doped Ag NCs, the compositions and structures of the nanoclusters have been investigated. The study of doped nanoclusters relies on their parent nanoclusters because they bear homologous structures. At the same time, the nature of the doped heteroatoms also plays a crucial role in tuning the structures and properties. Many promising metal atoms have been chosen and proved to be competent in tailoring Ag NCs, such as Au, Pt, Pd, Cu, *etc.*, and several representative species of M_xAg_{n-x} NCs have been identified.[8–15]

Although many important advances have been made for gold nanoclusters, silver and its doped NCs are still not well understood. It is challenging to synthesize stable Ag NCs due to the easy oxidation of Ag under the zero-valent state. The breakthrough came from Ag_{44} with a determined crystal structure.[16,17] Subsequently, some well determined Ag NCs with various stable sizes were prepared, such as Ag_{20},[18,19] Ag_{21},[19,20] Ag_{25},[21] Ag_{29}, (ref. 22) and so on. Meanwhile, significant advances have been achieved in recent studies, which focus on the hetero-metal atom doping of Ag NC templates. However, there are few reviews that focus on Ag and its doped NCs. In our previous review, we have summarized new advances in synthetic methods, new sizes, structural determination and properties of Ag NCs.[23] In addition, in our latest review, we discussed luminescent Ag NCs and PL enhancement strategies.[24] In this work, we will highlight some recent advances in foreign-atom doped Ag NCs with a focus on their synthesis and identified structures. Of note, in this review we only focus on bimetallic Ag NCs. Trimetallic Ag NCs are not included in this review. Moreover, we will discuss doping effects on their properties, including the location and stability (where the foreign atoms go: the surface or inside the kernel), the changes in the charge state, the PL enhancement and the improvement in catalytic activity and selectivity. Finally, we provide our perspectives.

2. Synthesis of doped silver bimetallic nanoclusters

The concept of doping emerging in the fields of metal nanoclusters has been clarified in previous reviews.[8–10] Herein, doped Ag NCs are identified as $M_xAg_{n-x}(SR)_m$ (M = Au, Pt, Pd, Cu, *etc.*). The synthesis methods can be classified into four categories: (1) co-reduction of mixed metal-complexes, such as one-pot reduction of Ag–SR and M–SR mixed complexes, where the parent silver complexes and hetero-metal complexes are simultaneously reduced in one pot by the reductant; (2) doping homo-metal clusters with foreign metal salts or complexes, *via* galvanic exchange and anti-galvanic exchange, where hetero-metal salts or complexes react with Ag NCs *via* a redox process, and hetero-metals take the place of some Ag atoms, forming alloys; (3) inter-cluster reactions, where the reactions between Ag NCs and foreign metal NCs introduce foreign metals into Ag NCs, generating Ag bimetallic NCs; (4) the ligand-exchange method, where the structures of Ag bimetallic clusters can be converted by their reaction with introduced ligands. Atomically precise doping provides convenience for studying the composition and structure evolution. In addition, the number and nature of doping hetero-metal atoms and their doping locations (including centre, inner shell and outer shell) are also crucial factors, which need to be seriously considered. Different heteroatoms provide different electronic and geometric structures and diverse properties. This section summarizes the doping of different heteroatoms into silver nanoclusters, mainly including dopants like Au, Pt, and Pd, and non-noble metal atoms like Cu, Ni and Cd.

According to the advances in Ag NCs, there are several typical Ag NC templates for preparing doped Ag NCs: the most famous types are based on Ag_{25}, Ag_{29} and Ag_{44}, and there a few studies that are also based on Ag_{20}, Ag_{21} and some other stable sizes. Here, we will summarize doped Ag NCs according to the doped foreign atoms. We have reviewed hetero-metal atom doped Ag NCs in Table 1.

Dongpo Song received his PhD degree in physics from the University of Science and Technology of China, and then he worked at Jiangsu University of Science and Technology and the University of Pittsburgh. He is currently an Associate Professor at the department of Applied Physics in Jiangsu University of Science and Technology. His research interest mainly lies in functional film materials, with a focus on growth mechanisms and electrical properties.

Prof. Man-Bo Li was born in Hubei, China, in 1986. He received his B.S. (2008) and PhD (2013) degrees from the University of Science and Technology of China, under the supervision of Prof. Shi-Kai Tian. After three years of research at the Chinese Academy of Sciences, a short stay at King Abdullah University of Science and Technology, and postdoctoral research at Stockholm University with Prof. Jan-E. Bäckvall (2017–2019), he started his independent academic career as a professor at Anhui University, China, in December of 2019. His current research interests focus on heterogeneous metal catalysis and nanocluster catalysis.

Table 1 Silver nanoclusters doped with various hetero-metal atoms

Dopants	Templates	Formula	Synthesis methods	Ref.
Au	Ag_{25}	$[Ag_{24}Au(2,4\text{-}SPhMe_2)_{18}]^-$	Galvanic reaction	26
		$[Au_1Ag_{24}(Dppm)_3(SR)_{17}]^{2+}$	Co-reduction	27
	Ag_{29}	$Au_1Ag_{28}(LA)_{12}{}^{3-}$	Co-reduction & galvanic reaction	28
		$Ag_{29-x}Au_x(BDT)_{12}(TPP)_4$	Co-reduction	29
		$[Au_4Ag_{23}(C{\equiv}CBu^t)_{10}(dppf)_4Cl_7](PF_6)_2$	Co-reduction	30
		$[Au_5Ag_{24}(C{\equiv}CC_6H_4\text{-}p\text{-}Bu^t)_{16}(dppf)_4Cl_4](PF_6)_3$	Co-reduction	30
	Ag_{44}	$[Ag_{32}Au_{12}(SR)_{30}]^{4-}$		17
		$M_4Au_xAg_{44-x}(p\text{-MBA})_{30}$	Co-reduction	31
		$Ag_{44-x}Au_x(SR)_{30}{}^{4-}$ $(x = 0\text{–}12)$.	Inter-cluster reaction	32
	Ag_{20}	$[Au_{1+x}Ag_{20-x}\{Se_2P(O^iPr)_2\}_{12}]^+$	Galvanic reaction	33
		$[AuAg_{19}\{S_2P(O^nPr)_2\}_{12}]$	Galvanic reaction	34
		$[Au@Ag_{20}\{S_2P(O^nPr)_2\}_{12}]^+$	Galvanic reaction	34
	Ag_{33}	$[Ag_{33}AuS_2(PhCH_2S)_{18}(CF_3COO)_9(DMF)_6]$	Co-reduction	35
	Giant sizes	$[Ag_{46}Au_{24}(SR)_{32}](BPh_4)_2$, $Ag_{267-x}Au_x(SR)_{80}$	Co-reduction	36 and 37
Pt	Ag_{25}	$[PtAg_{24}(SR)_{18}]^{2-}$	Galvanic reaction	38
		$Pt_2Ag_{23}Cl_7(PPh_3)_{10}$	Co-reduction	39
		$Pt_1Ag_{12}(dppm)_5(SPhMe_2)_2$	Ligand-exchange	40
	Ag_{29}	$[PtAg_{28}(BDT)_{12}(TPP)_4]^{4-}$	Ligand-exchange	42
		$PtAg_{28}(S\text{-}Adm)_{18}(PPh_3)_4$	Ligand-exchange & co-reduction	41 and 46
		$[PtAg_{28}(BDT)_{12}(PPh_3)_4]^{4-}$	Ligand-exchange	44
	Other sizes	$Pt_1Ag_{31}(S\text{-}Adm)_{16}(DPPM)_3Cl_3$	Galvanic reaction	47
		$[Pt_3Ag_{33}(PPh_3)_{12}Cl_8]^+$	Galvanic reaction	48
		$PtAg_{20}(dtp)_{12}$, $Pt_2Ag_{33}(dtp)_{17}$, $Pt_3Ag_{44}(dtp)_{22}$	Co-reduction	49
Pd	Ag_{25}	$[PdAg_{24}(SR)_{18}]^{2-}$	Co-reduction	25
	Ag_{29}	$[PdAg_{28}(S\text{-}Adm)_{18}(PPh_3)_4]^{2+}$	Co-reduction	50
	Ag_{21}	$[PdAg_{20}\{S_2P(O^nPr)_2\}_{12}]$	Co-reduction	51
		$[Pd_6Ag_{14}(S)\{S_2P(O^nPr)_2\}_{12}]$	Co-reduction	51
Cu		$[Ag_{28}Cu_{12}(SR)_{24}]^{4-}$	Co-reduction	52
		$[Ag_{61}Cu_{30}(SAdm)_{38}S_3]BPh_4$	Co-reduction	53
Ni	Ag_{25}	$[NiAg_{24}(SPhMe_2)_{18}]^0$, $[NiAg_{24}(SPhMe_2)_{18}]^{2-}$	Co-reduction	14
	Ag_{29}	$[NiAg_{28}(BDT)_{12}]^{4-}$, $[NiAg_{28}(BDT)_{12}]^{3-}$	Ligand-exchange	55
Cd		$Cd_{12}Ag_{32}(SePh)_{36}$	Co-reduction	54

2.1 Au doping

Silver and gold have nearly identical atomic radii, which are 2.89 and 2.88 Å, respectively. Gold is much more stable in the zero-valent state. Gold doped Ag NCs have been well studied and compared with their Ag NC analogue. The Au dopant can occupy both positions, *i.e.*, the centre core and the kernel shell.

$[Ag_{25}(SR)_{18}]^-$ was reported in 2015 by Osman M. Bakr *et al.*[21] At the same time, Zheng's group gave a report on homologous gold doped Ag NCs: $Ag_{24}M(SR)_{18}$,[25] and then Bakr *et al.* prepared $[Ag_{24}Au(2,4\text{-}SPhMe_2)_{18}]^-$ in 2016.[26] Zhu and his co-workers prepared $[Au_1Ag_{24}(Dppm)_3(SR)_{17}]^{2+}$, which contained 6 free valence electrons.[27]

This work bridges the gap in the understanding of 6e $Ag_{24}M(SR)_{18}$ NCs. As Ag_{25} fits the super atom model, there are two reasonable charges of $M@Au_{24}$: 0 or 2 charge states, which correspond to 6e and 8e, respectively. They synthesized this Au_1Ag_{24} *via* the co-reduction method, where Ag and Au ions were reduced in one pot. The formula has been identified as 1 Au and 24 Ag protected by 17 cyclohexyl mercaptan and 3 Dppm *via* ESI-MS measurements. The $[Au_1Ag_{24}(Dppm)_3(SR)_{17}]^{2+}$ contains open icosahedral Au_1Ag_{12} surrounded by a $Ag_{12}(Dppm)_3(SR)_{15}$ ring motif and two thiols, see Fig. 1A. In the Au_1Ag_{12} kernel, there is a distortion, which leads to longer Au–

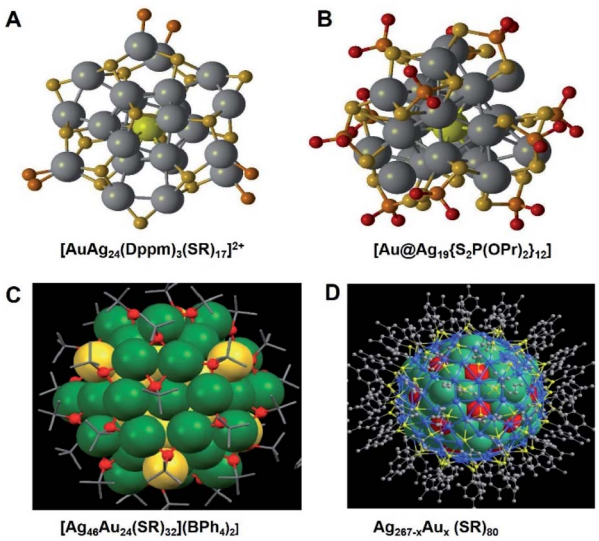

Fig. 1 Crystal structure of Au doped Ag Bimetallic NCs. Redrawn (A and B) and reproduced (C and D) from ref. 27, 34, 36 and 37. Copyright 2019 and 2018 Royal Society of Chemistry. Copyright 2015 American Association for the Advancement of Science. Copyright 2018 Springer Nature.

Ag and Ag–Ag bond lengths that range from 2.730 to 3.068 Å and from 2.851 to 2.982 Å, respectively.

There are more varieties of gold-doped Ag_{29} NCs, and they contain different numbers of surface ligands. Groot's group tried to synthesize $Au_1Ag_{28}(LA)_{12}{}^{3-}$ (LA = lipoic acid) *via* the co-reduction approach and galvanic reactions, and the products show a preference for mono-doped clusters.[28] In their work, they predicted the central location of the doped Au by X-ray absorption spectroscopy (XAS). Cui[29] and his co-workers prepared $Ag_{29-x}Au_x(BDT)_{12}(TPP)_4$ (x = 1–5), and they identified the reasonable substitution site of x Au by using DFT and TD-DFT calculations. Of note, according to the calculations, the energy barrier of center doping is about 10 kcal mol^{-1}, which is less than that of the others, matching the experimental results that it is the most stable one. They further discussed the crucial influences of the heteronuclear Au–Ag bonds on the electronic structures and optical performance. We will discuss the photoluminescence enhancement in the next section. In Wang's work,[30] they claimed that surface ligands play a vital role and can adjust the doping pattern in Ag alloy NCs. There was only a subtle change of groups between the two alkynyl ligands, which resulted in the formation of two entirely different bimetallic NCs: $[Au_4Ag_{23}(C{\equiv}CBu^t)_{10}(dppf)_4Cl_7](PF_6)_2$ and $[Au_5Ag_{24}(C{\equiv}CC_6H_4\text{-}p\text{-}Bu^t)_{16}(dppf)_4Cl_4](PF_6)_3$. The synthesis was carried out by the method of co-reduction. Au_4Ag_{23} and Au_5Ag_{24} have different geometric structures and electronic properties. They both have an icosahedral $Au@Ag_{12}$ core, and the outer motifs are $Au_3Ag_{11}(C{\equiv}CBu^t)_{10}(dppf)_4Cl_7$ in Au_4Ag_{23} and $Au_4Ag_{12}(C{\equiv}CC_6H_4\text{-}p\text{-}Bu^t)_{16}(dppf)_4Cl_4$ in Au_5Ag_{24}, respectively. The total number of valence electrons in Au_4Ag_{23} is eight, which belongs to the spherical superatomic series, while the $Au@Ag_{12}$ kernel of Au_5Ag_{24} is an oblate ellipsoid, and the number of valence electrons is 6, which can fit the electronic configuration $[S\sigma]^2[P\sigma]^4$. This work provides new insights into the unexpected role of the ligand in doping reactions.

The $Ag_{44}(SR)_{30}$ is the first reported Ag NC with a determined structure. In 2013, both Bigioni and Zheng reported the structure of $[Ag_{44}(p\text{-MBA})_{30}]^{4-}$ and $[Ag_{44}(SR)_{30}]^{4-}$ (SR = SPhF, $SPhF_2$, or $SPhCF_3$), respectively.[16,17] And in the same work of Zheng's group, several $[Ag_{32}Au_{12}(SR)_{30}]^{4-}$ (SR = SPhF, $SPhF_2$, or $SPhCF_3$) alloys have also been obtained.[17] Further, Bigioni *et al.*[31] have mapped the possible compositions of Ag alloy NCs which take $M_4Au_xAg_{44-x}(p\text{-MBA})_{30}$ (M = counteraction, x = 0–12) as the model, while other groups also reported the synthesis of $[Ag_{44-x}Au_x(SR)_{30}]^{4-}$ alloy NCs. In the work of Pradeep and his co-workers,[32] they prepared Au doped Ag NCs *via* an inter-cluster reaction between $Ag_{44}(SPhF_2)_{30}{}^{4-}$ and $Au_{25}(PET)_{18}{}^{-}$:

$$Ag_{44}(SPhF_2)_{30}{}^{4-} + Au_{25}(PET)_{18}{}^{-} \rightarrow Ag_{44-x}Au_x(SR)_{30}{}^{4-}\ (x = 0\text{–}12).$$

DFT calculations of the isomers of $Au_{12}Ag_{32}(SR)_{30}{}^{4-}$ confirm that the most stable isomer is the $Au_{12}@Ag_{32}$ (E = 0), where the Au occupies the centre positions of the kernel. These results also match those in the earlier studies.

Apart from the Au doped Ag NCs, by using the common Ag NC templates, several other stable sizes of Ag alloys have been reported. Liu *et al.* synthesized Ag_{20} and Ag_{21} NCs, where S and Se were used as donor ligands, respectively.[18–20] In their studies, they also reported alloys based on these Ag_{20} and Ag_{21} templates. They obtained $[Au_{1+x}Ag_{20-x}\{Se_2P(O^iPr)_2\}_{12}]^+$ (x = 0–2) alloy NCs by performing galvanic exchange on the $[Ag_{20}\{Se_2P(O^iPr)_2\}_{12}]$ template.[33] It's noteworthy that the first dopant Au leads to a metal nuclearity increase from 20 to 21, whereas subsequent Au-atom doping maintains the total number of metal atoms. This is different from the reported mechanism for Au doped Ag NCs we mentioned before. The single crystals of $[Au@Ag_{20}\{Se_2P(O^iPr)_2\}_{12}]^+$ and $[Au@Au_2Ag_{18}\{Se_2P(O^iPr)_2\}_{12}]^+$ were successfully obtained and their structures were determined. The $[Au@Ag_{20}\{Se_2P(O^iPr)_2\}_{12}]^+$ bears a T symmetry, which is similar to the $[AuAg_{20}\{Se_2P(OEt)_2\}_{12}]^+$ and $[Au@Au_2Ag_{18}\{Se_2P(O^iPr)_2\}_{12}]^+$ that possess C_1 symmetries, while their parent $[Ag_{20}\{Se_2P(O^iPr)_2\}_{12}]$ has a C_3 symmetry. There are two types of S-donor Au doping Ag alloys: $AuAg_{19}$ and $AuAg_{20}$.[34] Firstly, $[AuAg_{19}\{S_2P(O^nPr)_2\}_{12}]$ was prepared *via* a galvanic exchange route based on the Ag_{20} template, see Fig. 1B. And it was further transformed to higher nuclearity $[Au@Ag_{20}\{S_2P(O^nPr)_2\}_{12}]^+$ by reaction with Ag^+ salt at low temperature. These studies give a prospect for further study of core-size controlled preparation of the doped Ag NCs.

Zang's[35] group synthesized 3-electron Ag_{34} NCs and Au doped $Ag_{33}Au$ alloy NCs *via* the one-pot reduction method. $Ag_{33}Au$ has a similar framework to Ag_{34}, where the doping Au atom takes the place of the core Ag atom. However, $Ag_{33}Au$ showed vigorous stability compared to Ag_{34}. Furthermore, some larger sized Au doped Ag NCs have been reported, for instance, $Au_{24}Ag_{46}$ (ref. 36) and Au_xAg_{267-x},[37] see Fig. 1C and D. The $[Au_{24}Ag_{46}(SR)_{32}](BPh_4)_2$ contains a $Ag_2@Au_{18}@Ag_{20}$ kernel which is protected by a chiral $Ag_{24}Au_6(SR)_{32}$ outer shell.[36] Unlike the other $Ag_{n-x}Au_x(SR)_m$ alloy NCs we discussed above, the doped Au atoms didn't occupy the centre of the core of the $Au_{24}Ag_{46}$ NCs. The spherical $(AuAg)_{267}(SR)_{80}$ is generated with trigonal-prismatic $(AuAg)_{45}$(2,4-$SPhMe_2)_{27}$ (ratio 1 : 1) *via* co-crystallization. The $Ag_{267-x}Au_x(SR)_{80}$ (ref. 37) contains a four concentric-shell icosahedral structure of $Ag@M_{12}@M_{42}@M_{92}@Ag_{120}(SR)_{80}$ (M = Au or Ag) with I_h symmetry. The centre atom of the core is Ag, the same as that in the $[Ag_{46}Au_{24}(SR)_{32}](BPh_4)_2$.

2.2 Pt doping

Platinum doping in Ag NCs has been demonstrated to be feasible. According to the reported studies, most of the Pt–Ag alloys are synthesized based on the Ag_{25} and Ag_{29} templates.

Zheng *et al.* have synthesized a doped Ag NC $[MAg_{24}(SR)_{18}]^{2-}$, in which the dopant could be Pd or Pt.[38] They adopted and improved the one-pot synthesis method of $[Ag_{44}(SR)_{30}]^{4-}$, by adding $PdCl_2$ or K_2PtCl_4, to prepare $[MAg_{24}(SR)_{18}]^{2-}$. The $[MAg_{24}(SR)_{18}]^{2-}$ (M = Pd, Pt) NC bears a $M@Ag_{12}$ core capped by six distorted dimeric –RS–Ag–SR–Ag–SR– staple motifs, see Fig. 2A and B. Basset and his co-workers have synthesized a rod-like $Pt_2Ag_{23}Cl_7(PPh_3)_{10}$ *via* a one pot co-reduction method.[39] It contains two $PtAg_{12}$ icosahedra, which are self-assembled into a rod-shape by vertex-sharing, see Fig. 2C. Electronic structure calculations further illustrate the origin of Pt centre-doping-

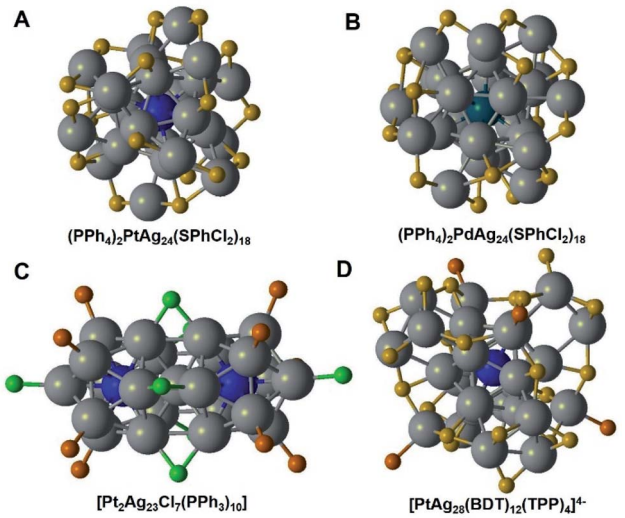

Fig. 2 Crystal structure of Pt (A, C and D) and Pd (B) doped Ag bimetallic NCs. Redrawn with permission of ref. 38, 39 and 42. Copyright 2015 and 2017 American Chemical Society. Copyright 2017 Royal Society of Chemistry.

dependent enhancement of stability. Zhu and his co-workers obtained $Pt_1Ag_{12}(dppm)_5(SPhMe_2)_2$ NCs by using the ligand-exchange method with $Pt_2Ag_{23}Cl_7(PPh_3)_{10}$.[40] After first etching with a HS–$PhMe_2$ ligand, $Pt_2Ag_{23}Cl_7(PPh_3)_{10}$ transformed to $PtAg_{24}(SPhMe_2)_{18}$, where the rod-like $PtAg_{12}$ icosahedra split into one $PtAg_{12}$ icosahedron capped with six $Ag_2(SR)_3$ dimeric motifs. After that, the $PtAg_{24}(SPhMe_2)_{18}$ NC was etched into a smaller mono-icosahedral $PtAg_{12}$ nanocluster by a dppm ligand. However, $PtAg_{12}$ NCs are not as stable as Pt_2Ag_{23} and $PtAg_{24}$, and it is difficult to obtain their single crystals. Wu's group reported a $PtAg_{26}(2\text{-}EBT)_{18}(PPh_3)_6$ alloy, in which a bipyramid $Pt@Ag_{14}$ kernel is surrounded by six dimeric (–SR–Ag–SR–Ag–PR_3–) staple motifs.[41] Both $PtAg_{26}$ and $PtAg_{24}$ are 8e superatoms, and they share highly similar electronic structures.

There are several studies that reported the synthesis of $PtAg_{28}$ NCs. Unlike Au_1Ag_{28} NCs, $PtAg_{28}$ NCs were prepared *via* the ligand-exchange approach and more kernel structure types were formed, including icosahedral and FCC structures. Basset *et al.* synthesized $[PtAg_{28}(BDT)_{12}(TPP)_4]^{4-}$ by the reaction of $Pt_2Ag_{23}Cl_7$ $(TPP)_{10}$ with a $BDTH_2$ (1,3-benzenedithiol) ligand.[42] The Pt dopant in $PtAg_{28}$ also occupies the center position of the icosahedron core. $PtAg_{28}$ possesses a closed-shell electronic configuration, showing enhanced stability, see Fig. 2D. Of note, they further doped Au atoms into these bimetallic NCs, and found out that the Au atom takes the place of the Ag atom, forming $[PtAuAg_{27}(BDT)_{12}]^{4-}$ trimetallic NCs. Kang *et al.*[43] prepared $PtAg_{28}(S\text{-}Adm)_{18}(PPh_3)_4$ NCs *via* etching $Pt_1Ag_{24}(SPhMe_2)_{18}$ with the 1-adamantanethiolate and triphenyl phosphine ligands. The Pt atom in the $PtAg_{28}(S\text{-}Adm)_{18}(PPh_3)_4$ also occupies the center position. This NC bears a face-centered cubic (FCC) $PtAg_{12}$ kernel, which is different from that of the doped Ag NCs that we discussed above. $PtAg_{28}(S\text{-}Adm)_{18}(PPh_3)_4$ exhibited better thermal-stability and stronger luminescence than $Pt_1Ag_{24}(SPhMe_2)_{18}$. In subsequent research, chemists tried to identify the relationship between the icosahedron and FCC structures. Bakr *et al.*[44] obtained $[PtAg_{28}(BDT)_{12}(PPh_3)_4]^{4-}$ NCs with a FCC structure by the ligand exchange method, using dithiolate 1,3-benzenedithiolate to replace the bulky mono-thiolate 1-adamantanethiolate in the icosahedron $[PtAg_{28}(S\text{-}Adm)_{18}(PPh_3)_4]^{2+}$. Zhu and his co-workers[45] reported the reversible transformation between the icosahedral and FCC structures: the 1-adamantanethiolate capped $PtAg_{28}$ with a FCC kernel was transformed to its isomer with an icosahedral kernel in the presence of cyclohexanethiolate. Interestingly, the reverse process was also observed by the addition of 1-adamantanethiolate. In the latest work of Huang's group,[46] they synthesized $[PtAg_{28}(S\text{-}Adm)_{18}(PPh_3)_4]^{2+}$ by a one-pot wet chemical method. It was a breakthrough in preparing $PtAg_{28}$ alloy NCs. Compared with the previous ligand-exchange method, they achieved high symmetry with the FCC kernel in high yield.

Although most of the studies on Pt doped Ag NCs are based on templates of Ag_{25} or Ag_{29}, some other sized Pt–Ag alloy NCs were investigated as well. Kang *et al.*[47] prepared $Pt_1Ag_{31}(S\text{-}Adm)_{16}(DPPM)_3Cl_3$ *via* the reaction between $Pt_1Ag_{28}(SAdm)_{18}(PPh_3)_4$ and $Ag_2(DPPM)Cl_2$ complexes. The $Ag_2(DPPM)Cl_2$ substitutes the Ag–PPh_3 units, leading to the size growth of the NCs. Although it maintains the same composition as the Pt_1Ag_{12} kernel, the FCC configuration in the Pt_1Ag_{28} changes to an icosahedral configuration. The Pt_1Ag_{12} kernel is protected by a three $Ag_6(SR)_6(DPPM)Cl$ assembly *via* sharing $Ag_2(SR)_3$ edges. $Pt_1Ag_{31}(S\text{-}Adm)_{16}(DPPM)_3Cl_3$ exhibited a different UV absorption compared to $Pt_1Ag_{28}(SAdm)_{18}(PPh_3)_4$, so it is easy to distinguish them. $[Pt_3Ag_{33}(PPh_3)_{12}Cl_8]^+$ with three icosahedral $PtAg_{12}$ building blocks, where adjacent $PtAg_{12}$ units share a vertex with silver atoms in a cyclic manner, was reported by Zhu's group.[48] It can be classified as the same homologous series with rod-like $Ag_{23}Pt_2Cl_7(PPh_3)_{10}$ and $Pt_1Ag_{12}(dppm)_5(SPhMe_2)_2$ NCs. It exhibits growing evolution from single icosahedral $PtAg_{12}$ to rod-like bi-icosahedral $PtAg_{12}$, and then to a cyclic tri-icosahedral $PtAg_{12}$. Comparing the UV absorption and PL excitation of Pt_3Ag_{33} with those of Pt_1Ag_{12} and Pt_2Ag_{23}, it was found that there is a continuous red shift with the assembly of more $PtAg_{12}$ units. Furthermore, Liu and his co-workers[49] obtained three bimetallic Pt doped Ag NCs: $PtAg_{20}(dtp)_{12}$, $Pt_2Ag_{33}(dtp)_{17}$, and $Pt_3Ag_{44}(dtp)_{22}$ (dtp: dipropyl dithiophosphate) *via* the one pot co-reduction approach, which are 8e, 16e and 22e super molecules, respectively. Similar to Pt_1Ag_{12}, Pt_2Ag_{23} and Pt_3Ag_{33}, these three homoleptic $PtAg_{20}(dtp)_{12}$, $Pt_2Ag_{33}(dtp)_{17}$, and $Pt_3Ag_{44}(dtp)_{22}$ contain one, two and three centered icosahedral $Pt@Ag_{12}$ units, respectively. $Pt_2Ag_{33}(dtp)_{17}$ with 16 electrons contains two noninteracting 8-electron vertex-sharing icosahedral super molecules, and its electronic structure is isolobal to Ne_2. The $Pt@Ag_{12}$ units in $Pt_3Ag_{44}(dtp)_{22}$ are assembled linearly by vertex-sharing, and its electronic structure is isolobal to the triiodide ion. These inter-icosahedral bonding interactions provide evidence and chances for deeper understanding and further investigation of super molecular alloys.

2.3 Pd doping

Similar to Pt doped Ag NCs, palladium doped Ag NCs are usually prepared based on Ag_{20}, Ag_{25} and Ag_{29} NCs, and the Pd dopant

also prefers center doping. As we discussed above, Zheng's group[25] used the one pot method to prepare $[PdAg_{24}(SR)_{18}]^{2-}$. It has a centred icosahedral $Pd@Ag_{12}$ core stabilized by six distorted dimeric staple –RS–Ag–SR–Ag–SR– motifs, which is similar to $Au_{25}(SR)_{18}$. They carefully compared the structures of $[PdAg_{24}(SR)_{18}]^{2-}$ and $Au_{25}(SR)_{18}$, and found that there were several distortions in $PdAg_{24}$. Moreover, the distorted dimeric staple motifs change the surface chemical environment. Due to the interactions between neighbouring staple units on the surface, they bear shorter Ag…S distances (3.006 Å in average) than $Au_{25}(SR)_{18}$. Therefore, the structure of $[PdAg_{24}(SR)_{18}]^{2-}$ can be considered as an icosahedral $Pd@Ag_{12}$ core capped by four triangular surface $[(AgSR)_3(SR)_{3/2}]$ units.

Huang *et al.*[50] prepared $[PdAg_{28}(S\text{-}Adm)_{18}(PPh_3)_4]^{2+}$ with a FCC kernel surrounded by a tetrahedron-like $Ag_{16}S_{18}P_4$ shell *via* the one pot approach. The outer shells contain four $Ag_4S_6P_1$ staple motifs sharing six S, which is the same as that of the $PtAg_{28}$ we mentioned above. Of note, $PdAg_{28}$ reacted with $AuPPh_3Cl$, forming $AuAg_{28}$ bimetallic NCs instead of trimetallic alloy NCs. This observation is quite different from that of the reaction between $PtAg_{28}$ and the Au complex. Liu[51] and his co-workers prepared $[PdAg_{20}\{S_2P(O^nPr)_2\}_{12}]$ based on the $[Ag_{21}\{S_2P(O^iPr)_2\}_{12}]^+$ template, by the co-reduction method. It has an 8e $[PdAg_{12}]^{4+}$ superatomic core capped by eight Ag^+ in C_2 symmetry. DFT calculations show that the center displacement energy of Pd is more than 20 kcal mol^{-1} that of other positions. Moreover, they obtained $[Pd_6Ag_{14}(S)\{S_2P(O^nPr)_2\}_{12}]$ by increasing the amount of $[Pd\{S_2P(O^nPr)_2\}_2]$. Its structure is completely different from $PdAg_{20}$, even though they exist in the reaction solution at the same time. The $[Pd_6Ag_{14}(S)\{S_2P(O^nPr)_2\}_{12}]$ has a sulfide-centered Pd_6Ag_2 rhombohedron core capped by twelve silver atoms with S_6 symmetry, and it displays a smaller electrochemical HOMO–LUMO gap. Compared with the common icosahedron or FCC core, this octahedral hexa-palladium(0) kernel embedded within a silver(I) cluster is a novel structure type in alloy NCs.

2.4 Cu doping

Cu(0) nanoclusters are rarely reported due to their easy oxidation. There is only a little preliminary progress on copper doped Ag NCs. Zheng's group reported the first Ag–Cu bimetallic alloy, $[Ag_{28}Cu_{12}(SR)_{24}]^{4-}$.[52] It has a chiral metal framework with T symmetry, and its kernel is arranged in a three-concentric shell structure composed of $Ag_4@Ag_{24}@Cu_{12}(SR)_{24}$, where a two-shell $Ag_4@Ag_{24}$ core is capped by four nearly planar $Cu_3(SR)_6$ staple motifs, see Fig. 3A. The Cu atoms take the place of the Ag atoms in the outer shell, and these 28 Ag atoms are arranged in a distorted FCC pattern, which results in a distorted HCP Ag–Cu interface. Its chiral separation and asymmetric synthesis was conducted by ion pairing with chiral quaternary ammonium salts. In the synthesis process, they used achiral counter cations ($^nBu_4N^+$), and hence the as-prepared cluster was a racemic mixture. Furthermore, this racemic mixture can be separated into enantiomers by using chiral quaternary ammonium salts, such as *N*-benzylcinchonidinium chloride (BCDC) and *N*-benzylcinchoninium chloride (BCNC), thereby obtaining optically pure enantiomers separately. This asymmetric synthesis and ion paring chiral enantio-separation provides effective routes for preparing chiral metal NCs.

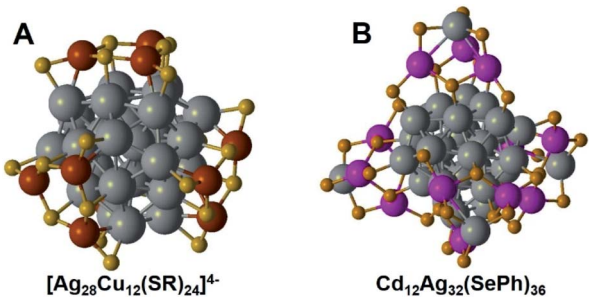

Fig. 3 Crystal structure of Pd (A) and Cd (B) doped Ag Bimetallic NCs. Redrawn with permission of ref. 52 and 54. Copyright 2016 and 2019 American Chemical Society.

Zhu's[53] group reported kernel-doping of Cu atoms in Ag NCs, and the preparation of a giant bimetal NC $[Ag_{61}Cu_{30}(SAdm)_{38}S_3]BPh_4$ which possesses a rare valence of 46 free electrons. $Ag_{61}Cu_{30}$ ($Ag_{13}@Cu_{30}@Ag_{48}(SAdm)_{38}S_3$) also has a three-shell framework, where the Cu_{30} is in the middle layer. The icosahedral Ag_{13} kernel is enclosed by a Cu_{30} icosidodecahedron, where each Ag atom connects five pentagonal Cu atoms, and is further capped by an $Ag_{48}(SAdm)_{38}S_3$ outer shell. Doping active metal atoms in the kernel of metal NCs offers new insights into the atomically controlled synthesis of metal alloy NCs.

2.5 Other hetero-metal doping

Apart from the above-mentioned Ag alloy nanoclusters doped with Au, Pt, Pd and Cu, several other metal doped Ag alloy NCs, such as Ni and Cd doped Ag alloy NCs, were also reported.

Hyeon and Zheng *et al.*[54] reported a Cd doped Ag nanocluster $Cd_{12}Ag_{32}(SePh)_{36}$ by a phosphine-assisted process, see Fig. 3B. Cd occupied the outer shell positions, and formed an asymmetric two-shell $Ag_4@Ag_{24}@Cd_3Ag(SePh)_9$ framework. The $Ag_4@Ag_{24}$ kernel contains a Ag_4 tetrahedron, which is encapsulated by four Ag_6 facets. This Ag_{28} kernel in $Cd_{12}Ag_{32}(SePh)_{36}$ is similar to the core in $[Cu_{12}Ag_{28}(SR)_{24}]^{4-}$.[52] In the outer layer of $Cd_3Ag(SePh)_9$, there are three $CdSe_4$ tetrahedra, where three Se bind with one Ag to form a $AgSe_3$ cap-like structure. According to the electronic structure analysis and DFT calculations, it is a 20e superatom, which exhibits a chiral optical response.

Ni doped Ag NCs were synthesized based on Ag_{25} and Ag_{29}. The synthesis of $NiAg_{24}$ (ref. 14) was carried out by the co-reduction method while the $NiAg_{28}$ (ref. 55) was prepared by the ligand-exchange method. For $NiAg_{24}$, they obtained a neutral 6e $[NiAg_{24}(SPhMe_2)_{18}]^0$ and an 8e $[NiAg_{24}(SPhMe_2)_{18}]^{2-}$. The neutral $NiAg_{24}$ is much more stable than the dianionic form. The crystal structure of $[NiAg_{24}(SPhMe_2)_{18}]^{2-}$ is determined to contain a centered icosahedral $NiAg_{12}$ core surrounded by six SR–Ag–SR–Ag–SR staple motifs. This structure is similar to the Pt and Pd doped MAg_{24}. For $NiAg_{28}$,[55] the ESI analysis suggested two molecules with different charge states: $[NiAg_{28}(BDT)_{12}]^{4-}$ and $[NiAg_{28}(BDT)_{12}]^{3-}$. In this work, Pradeep *et al.* also prepared

$[NiAg_{24}(DMBT)_{18}]^{2-}$. However, these Ni–Ag alloy NCs were less stable than their parent Ag NCs. Further work focusing on the preparation of stable Ni doped Ag NCs and understanding their geometric and electronic structures is needed.

3. Doping effects on properties

As we discussed in our previous studies, Ag NCs exhibit relatively poor stability compared to Au NCs, which makes their further study and applications challenging. Doping methods have been demonstrated to be efficient in tuning the properties of Ag NCs. The doping of Ag NCs with hetero atoms brings changes in constituent structure and electronic structure, which further influence their properties including PL, catalytic activity, chirality, *etc.*[7,8]

3.1 Doping location and stability

The atoms of Au, Pt, Pd, Cu and Ni have been doped into the NCs of Ag_{20}, Ag_{21}, Ag_{25}, Ag_{29} and Ag_{44}, *etc.* In general, most of the hetero atom doped Ag NCs exhibit enhanced stability compared to their parent Ag NCs. Bakr *et al.* showed that the $[Ag_{24}Au(SR)_{18}]^-$ undergoes minimal degradation in five days under ambient conditions, while pure Ag_{25} suffers obvious degradation after 24 h.[56]

Benefiting from the better stability, many Ag alloy NCs are reported with a determined crystal structure. The crystal structures of these doped Ag alloy NCs were studied using a single crystal X-ray diffractometer (SC-XRD). Different dopants prefer to occupy different locations in the Ag kernel due to their unique nature, see Fig. 4. Studying the reported structures of these Ag alloy NCs, we find some rules in doping locations. The Pt, Pd and Ni heteroatoms prefer to occupy the centre core position, while Au sometimes occupies the outer shell positions in giant Ag alloy NCs. For instance, the Au doped Ag alloy NCs $Ag_{46}Au_{24}(SR)_{32}](BPh_4)_2$[36] contain a $Ag_2@Au_{18}@Ag_{20}$ kernel. And the centre position is also occupied by a Ag atom in the $Ag_{267-x}Au_x(SR)_{80}$ NC kernel. Unlike the relatively stable noble metals, the Cu dopant is very active, and centre doping is full of challenges. Accordingly, Cu prefers to occupy the outer shell positions. In the case of $[Ag_{28}Cu_{12}(SR)_{24}]^{4-}$,[52] its kernel is arranged in a three-concentric shell framework composed of $Ag_4@Ag_{24}@Cu_{12}(SR)_{24}$, and the Cu atoms occupy the outermost shell to protect the two $Ag_4@Ag_{24}$ kernels. For $[Ag_{61}Cu_{30}(SAdm)_{38}S_3]BPh_4$,[53] Cu_{30} is arranged in the middle layer of the kernel, which is connected with the icosahedral Ag_{13} kernel and outer shell $Ag_{48}(SAdm)_{38}S_3$.

Density functional theory (DFT) calculations and the TD-DFT method were used to study the geometric and electronic structures and further theoretically validate the optimal location of the dopants in the Ag alloy nanocluster. Dolg and Cui *et al.*[29] studied the structures of $Ag_{29-x}Au_x$ ($x = 1$–5) NCs with possible isomers by performing DFT calculations. In their work, they claim that the Au atom prefers to occupy the central position. For instance, in the case of $x = 1$, the most stable isomer is the one in which Au is located in the central Ag_{13} icosahedral core. And when $x = 2$, the most stable isomer is the one in which two Au dopants occupy the central and vertical positions. Furthermore, they found that the $Ag_{29-x}Au_x$ ($x = 1$–5) NCs exhibit increased stability with the increase of Au–Ag bonds. In the work of Basset *et al.*,[42] they used TDDFT UV-vis spectra to analyze the optimal location of Pt in the $[PtAg_{28}(BDT)_{12}(P(CH_3)_3)_4]^{4-}$ NC, see Fig. 5A. They compared the simulated curves of $PtAg_{28}$ with different Pt locations based on the experimental spectrum. Accordingly, the Pt center doped curve is well matched with the experimental spectrum as they have similar main peaks and no low-energy features. The center doped $[PtAg_{28}(BDT)_{12}(P(CH_3)_3)_4]^{4-}$ NC shows higher thermodynamic stability. In Kappes's work, they monitored the reaction process *via* high-resolution trapped ion mobility mass

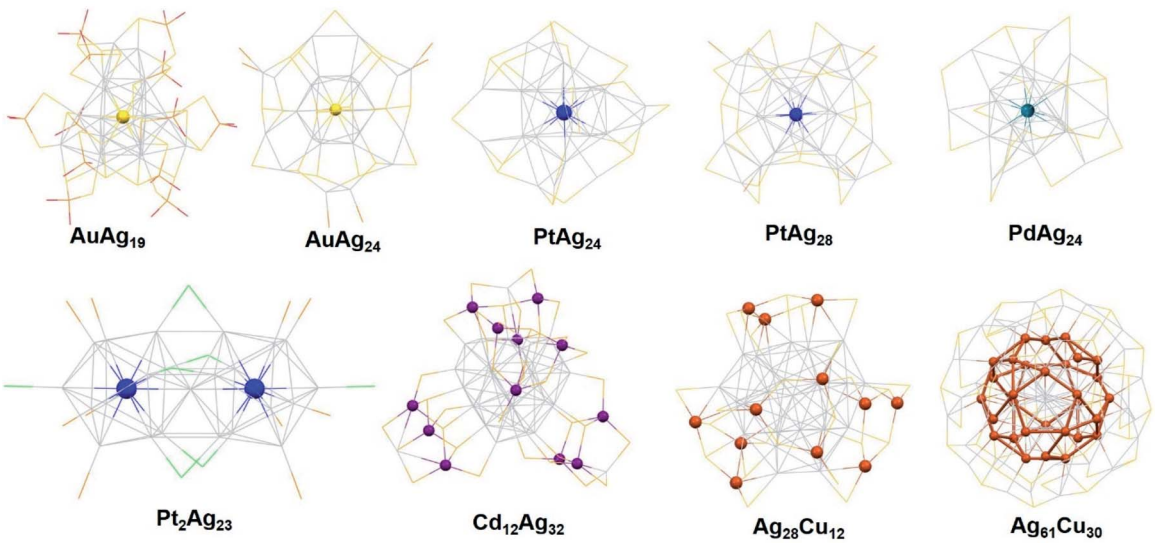

Fig. 4 Dopant locations in the crystal structures of hetero atom doped Ag Bimetallic NCs. Redrawn with permission of ref. 27, 34, 38, 42, 49, 52, 53 and 54. Copyright 2017, 2018 and 2019 Royal Society of Chemistry. Copyright 2015, 2016, 2017, 2019 and 2020 American Chemical Society.

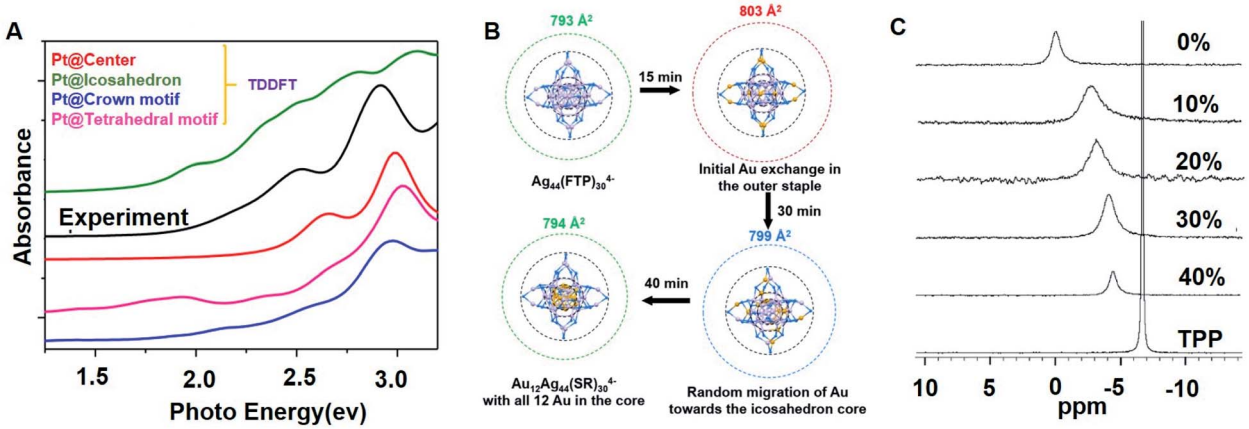

Fig. 5 (A) TDDFT UV-vis spectra of $[PtAg_{28}(BDT)_{12}(P(CH_3)_3)_4]^{4-}$ NCs for different Pt positions compared with the experimental spectrum. (B) Schematic of Au atom migration from the outer staple to the inner core. (C) NMR spectra of pure TPP, $Ag_{29}(BDT)_{12}(TPP)_4$, and $Ag_{29-x}Au_x(BDT)_{12}(TPP)_4$ clusters. Reproduced with permission of ref. 42, 32 and 56. Copyright 2019 American Chemical Society. Copyright 2017 Royal Society of Chemistry. Copyright 2016 Wiley-VCH.

spectrometry (TIMS), and they figured out the doping path of the gold atoms,[32] see Fig. 5B. Firstly, Au atoms displace Ag atoms in the outer staples of $Ag_{44}(SPhF_2)_{30}^{4-}$ and further migrate to the icosahedron core. At the same time, they theoretically analyzed the isomeric structures and collision cross section (CCS) values *via* DFT calculations and trajectory method calculations, respectively. They claimed that the most stable isomer is the centre doped $Au_{12}Ag_{32}(SR)_{30}$ based on the DFT calculations. In addition to the approach we mentioned above, the extended X-ray absorption fine structure (EXAFS) and the X-ray absorption near edge structure (XANES) methods were used in combination with electronic structure calculations to confirm the location of the Au dopants in the Au-doped Ag_{29} clusters.[28] And NMR measurements were also used to predict the Au location in the $Ag_{29}(BDT)_{12}(TPP)_4$ cluster,[56] see Fig. 5C. Overall, the SC-XRD, TIMS, EXAFS, XANES, DFT and TD-DFT methods were used to analyze the crystal structures of the Ag alloy NCs, which provide experimental and theoretical evidence to understanding the doping process. Although several structures of the Ag alloy NCs have been reported, further studies still need to focus on the preparation of Ag alloy NCs with more stable sizes and new types of dopants.

3.2 Charge state

Metal atoms show peculiarity in their outer electron arrangements and activities. Take Au and Ag as examples, both of them contain a single electron in the outermost S orbital. However, they exhibit different charge states: Ag exhibits the 1+ charge state, while Au exhibits 1+ or 3+ charge states. The addition of dopant hetero metal atoms would affect the electron cloud density and direction, and the value of the wave function would need to be recalculated. Therefore, doping would induce charge stripping and lead to diverse valence states. The $[Ag_{25}SR_{18}]^-$ NCs exhibit four charge states after doping with different foreign metal atoms, including 1−, 0, 2− and 2+. The Au doped $Ag_{25}SR_{18}$ alloy NCs display 1− and 2+ charge states: $[Ag_{24}Au(SPhMe_2)_{18}]^-$ and $[Au_1Ag_{24}(Dppm)_3(SR)_{17}]^{2+}$, see Scheme 1.[27] And with the Pt and Pd dopants,[38] a 2− charge state is seen: $[MAg_{24}(SR)_{18}]^{2-}$ (M = Pd, Pt). With the Ni dopant, 0 and 2− charge states of the NCs (neutral 6e $[NiAg_{24}(SPhMe_2)_{18}]^0$ and 8e $[NiAg_{24}(SPhMe_2)_{18}]^{2-}$) were obtained,[14] see Scheme 1. In the case of Ag_{29} cluster templates, three charges, 2+ 3− and 4−, were observed. The charge state remains at 3− after Au doping, while Pt doping alters the charge state to 2+ or 4− ($[PtAg_{28}(S\text{-}Adm)_{18}(PPh_3)_4]^{2+}$ and $[PtAg_{28}(BDT)_{12}(TPP)_4]^{4-}$).[42,45,46] Pd doping results in a 2+ charge state, $[PdAg_{28}(S\text{-}Adm)_{18}(PPh_3)_4]^{2+}$,[50] and Ni would convert the charge state to 4− or maintain at 3−: $[NiAg_{28}(BDT)_{12}]^{4-}$ and $[NiAg_{28}(BDT)_{12}]^{3-}$.[55] In the $Ag_{44}(SR)_{30}$ template, the charge state remains the same. The charge states of Ag_{20} and Ag_{21} are illustrated in Scheme 1. Doping reduced charge stripping will bring more opportunities in their reaction activities. What we need to consider is how to understand the mechanisms and further explain the charge stripping.

3.3 PL properties

The most anticipated property of silver nanoclusters is their photoluminescence (PL) property. However, considering their further application in a wide range of fields, there is an urgent

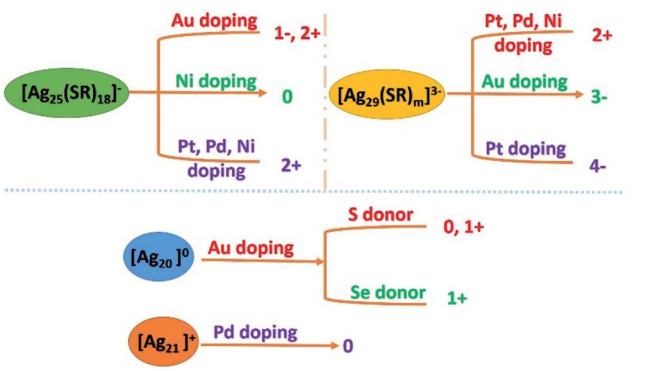

Scheme 1 Doping-induced charge stripping of $[Ag_{25}(SR)_{18}]^-$, $[Ag_{29}(SR)_m]^{3-}$, $[Ag_{20}]^0$, and $[Ag_{21}]^+$.

need for the synthesis of NCs with high quantum yield (QY) and long life. We have discussed the strategies for enhancing the luminescence of Ag NCs in our latest review; these properties are governed by their constitutions and structures.[24] There are two ways to improve the PL performance: modifying the metal kernel or tailoring the surface ligands. Doping is one of the most proven methods to improve the PL performance of Ag NCs. Bakr *et al.*[56] synthesized $Ag_{29-x}Au_x(BDT)_{12}(TPP)_4$ ($x = 1$–5) NCs by doping Au into $Ag_{29}(BDT)_{12}(TPP)_4$ clusters. The Au doped Ag_{29} clusters achieved 26-fold PL QY enhancement, from 0.9% (Ag_{29}) to 19% (30% Au dopants) and 24% (40% Au dopants).

Cui *et al.*[29] employed fs–ns TA spectroscopy to explore the electronic origins of PL enhancement. According to the TA spectra, there is an obvious shift in the GSB position at 435 nm for the Au doped Ag_{29} clusters. Moreover, the ESA curve displayed a change in the range of 485–800 nm after Au doping. Unlike the parent Ag_{29} NCs, after Au doping, the alloy shows improved time constants, where doping brings a longer lifetime, up to 612.65 ns (20% Au dopants) and 890.71 ns (40% Au dopants). The PL enhancement of the clusters depends on the nature of the excited state (S_1), which is highly affected by the doping amount of the Au atoms, see Fig. 6A. They used DFT and TD-DFT methods to explore the origin of the PL enhancement of Au doped $Ag_{29-x}Au_x$ ($x = 1$–5) clusters, in the lowest S_1 and S_0 electronic states. Generally, when the doping number of Au is 1 or 2, the PL performance of the $Ag_{29-x}Au_x$ clusters is very close to that of the undoped Ag_{29} cluster. When it is highly doped, with the doping number of Au going up to more than 3, there is an obvious increase in the PL intensity. This reveals that the crucial effects on the PL enhancement originate from Au dopants. Furthermore, they figured out that the Au–Ag bond played an important role in increasing the stability and governing the PL intensity. However, the Au amount effects cannot be generalized. In Mattoussi's work, the PL intensity does not simply increase with the increase of Au amount.[57]

Pt doped Ag NCs also exhibit a noticeable PL enhancement. Basset *et al.* reported an ~2.3 fold PL intensity increase in Pt

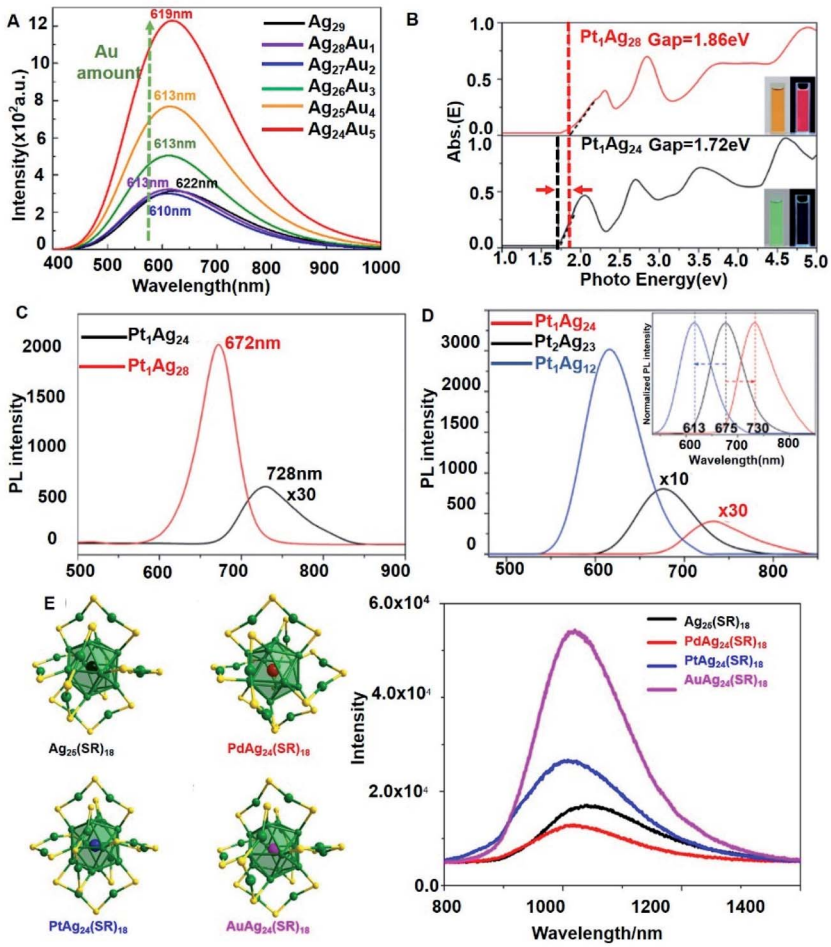

Fig. 6 (A) TD-DFT computed emission spectra of $Ag_{29-x}Au_x$ ($x = 0$–5) nanoclusters. (B and C) The spectra on the energy scale (B) and PL (C) of the Pt_1Ag_{24} and Pt_1Ag_{28} NCs. Insets show (B): digital photographs of each nanocluster in CH_2Cl_2 solution under visible and UV light. (D) The PL spectra of the Pt_2Ag_{23}, Pt_1Ag_{24} and Pt_1Ag_{12} nanoclusters. Inset: the peak shifts in normalized PL spectra. (E)Structures and photoluminescence spectra of $MAg_{24}(SR)_{18}$ (M = Ag/Pd/Pt/Au) NCs in the crystal state. Adapted with permission from ref. 29, 43, 40 and 58. Copyright 2018 Wiley-VCH. Copyright 2017 Royal Society of Chemistry. Copyright 2017 American Chemical Society.

doped Ag_{29} NCs, $[PtAg_{28}(BDT)_{12}(TPP)_4]^{4-}$.[42] Moreover, an ~80 nm red shift of the PL peak with broadening appeared after doping, where the broadening was attributed to the partial replacement of TPP ligands with solvent DMF molecules. They highlighted the solvent-effect on PL enhancement of the $PtAg_{28}$ alloy, whose surface was exposed to the solvent. In Zhu's work,[43] they obtained $Pt_1Ag_{28}(SR)_{18}(PPh_3)_4$ by the ligand exchange method based on $Pt_1Ag_{24}(SPhMe_2)_{18}$. They compared the energy scales and PL of these two alloy NCs, see Fig. 6B and C. The energy gaps of Pt_1Ag_{24} and Pt_1Ag_{28} are 1.72 eV and 1.86 eV, respectively. Moreover, the solution color of Pt_1Ag_{24} is green whereas that of Pt_1Ag_{28} is orange, and the PL of Pt_1Ag_{28} can be observed by the naked eye under UV light in the dark. In addition, the QYs of these two Pt doped Ag NCs are very different: the QY of Pt_1Ag_{24} is only 0.1% while that of Pt_1Ag_{28} is up to 4.9% (about a 50-fold enhancement). The PL peak of Pt_1Ag_{24} is at 728 nm, and it shifts to 672 nm when the Pt_1Ag_{28} is formed. They also compared the energy gaps and the PL spectra of $Pt_1Ag_{12}(dppm)_5(SPhMe_2)_2$, $Pt_1Ag_{24}(SPhMe_2)_{18}$ and $Pt_2Ag_{23}(PPh_3)_{10}Cl_7$.[40] The PL emission of Pt_2Ag_{23} is at 675 nm, while it shifted to 730 nm and 613 nm when it was converted to Pt_1Ag_{24} and Pt_1Ag_{12}, respectively, see Fig. 6D. Blue-shifts appeared in Pt_2Ag_{23} and Pt_1Ag_{24} when they were converted to Pt_1Ag_{12}, which can be assigned to the increase of the optical energy gap. However, the red shift of the PL emission on the conversion of Pt_2Ag_{23} to Pt_1Ag_{24} points out that the energy gap cannot fully represent the energy of PL due to the dramatic electronic perturbation and high vibration loss. Moreover, the PLQY displays a 28 times increase from 0.2 to 5.5% by re-assembling from Pt_2Ag_{23} to Pt_1Ag_{12}. The PL spectra of Pt_1Ag_{28} with different kernel structures (FCC and icosahedron) are very similar.[45] The PL QY of Pt_1Ag_{28} (icosahedron) is only 2.7% at room temperature, while that of Pt_1Ag_{28}(FCC) is 4.9%. However, the PL of Pt_1Ag_{28} (icosahedron) is temperature-dependent. It emits bright-red light at low temperature, and the QY reaches 100% at 98 K or lower temperature. Moreover, the PL intensity increases dramatically at low temperature.

Wu and his co-workers[58] studied a series of $MAg_{24}(SR)_{18}$ NCs, which were doped with different hetero atoms: Au, Pt and Pd. They compared the PL spectra of these Ag alloy NCs, see Fig. 6E. The Au doped $MAg_{24}(SR)_{18}$ showed the highest PL intensity.

To sum up, heteroatoms play a positive role in tuning the PL properties of Ag NCs. Doping leads to an obvious enhancement in the PL intensity and QY. It would provide various opportunities to their potential applications in the fields of bio-labelling, biomedicine, ion probing and so on. To synthesize and modify these functional alloy Ag NCs at the atomically precise level, we need to figure out the PL mechanism and the origin of PL enhancement. In previous studies, the origin of the PL enhancement was investigated *via* TA spectroscopy and DFT and TD-DFT methods. To date, the PL mechanism still needs deeper investigation. As we discussed above, many features can influence the PL performance, such as the dopant species, the doping amount, the alloy kernel structures, the solvent, the temperature and so on. However, the effects cannot be explained with a unified mechanism. Further study needs to focus on the fundamental PL mechanisms of these alloy NCs.

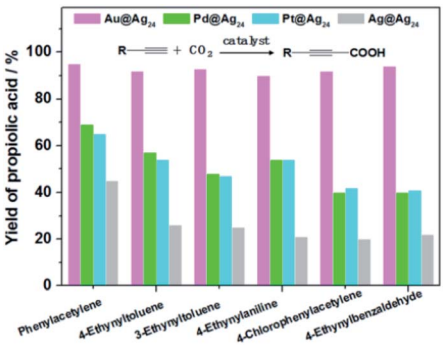

Fig. 7 The catalytic carboxylation of terminal alkynes with CO_2 over $Au@Ag_{24}$, $Pd@Ag_{24}$, $Pt@Ag_{24}$ and $Ag@Ag_{24}$ clusters, respectively. Adapted with permission from ref. 59. Copyright 2018 Wiley-VCH.

3.4 Catalytic properties

As we discussed above, doping tunes the electronic structure of Ag NCs and influences their catalytic properties. Zhu's group studied the catalytic performance of CNT-supported metal nanoclusters $Au_{24}Ag_{46}$ NC.[36] Compared with undoped NCs, this bimetallic $Au_{24}Ag_{46}$ NC takes advantage of both silver (high selectivity for benzaldehyde) and gold (high conversion) and showed higher conversion and selectivity for epoxides.

Zhu *et al.*[59] carried out centre doping of Ag_{25} NCs with different foreign atoms (Au, Pt and Pd), and further studied their influence on the catalytic performance in the carboxylation reaction of terminal alkynes with CO_2, see Fig. 7. The doping atoms indeed contribute to the catalytic properties, and the enhancement factors depend on the nature of the foreign atoms. The elegant work from Zhu and co-workers revealed the crucial structure of the Au@Ag kernel of the $Au_1Ag_{24}(SR)_{18}$ NC, which showed high activity and stability in catalyzing CF_3-ketone alkynylation. Their further studies demonstrated that the $Au_{12}Ag_{32}(SR)_{30}$ NCs, bearing a Au@Ag kernel, also showed high-activity, which confirmed their conclusion.[61] In Qin's work,[60] CeO_2 supported $Au_{13}Ag_{16}L_{24}$ NCs showed high catalytic activity and selectivity to A^3-coupling reactions. In all, the doped Ag NCs show great potential for catalytic application, where the dopants enhance the catalytic activity and selectivity. DFT calculations help to analyse the effect of the dopants on the catalytic process and understand the improvement factors.

4. Conclusions and outlook

In conclusion, we have summarized the recent studies on tailoring Ag NCs *via* doping with hetero metal atoms. Doping is based on Ag NC templates, and classified by the dopants: Au, Pt, Pd, Cu and other hetero atoms. The synthetic methods and the structures of bimetallic Ag NCs are highlighted. Furthermore, the doping effects on the properties of Ag NCs have been concluded, including the location of dopants, charge states, PL properties and catalytic properties. Doping improves or diversifies the properties of Ag NCs, providing versatile opportunities for their applications.

For future perspectives, we outline the following aspects:

(1) To date, only a few sizes of Ag bimetallic NCs have been reported, and these reports are mainly concentrated upon the templates of Ag_{25} and Ag_{29}. Studies on trimetallic Ag NCs are scarcer. The synthesis methods for preparing hetero atom doped Ag NCs are limited, and most of them are carried out by the ligand exchange approach. Exploring facile synthesis methods for preparing new sizes of doped Ag NCs is required.

(2) Although the locations of doping atoms have been analysed *via* SCXRD measurements and DFT calculations and the diffusion process has been monitored by using *in situ* UV-vis absorption spectroscopy in combination with ESI mass and tandem mass spectrometry,[62] the fundamental physical mechanisms are not well understood. To control the doping location and design doped Ag NCs with atomic precision, the occupation mechanism needs to be further studied.

(3) As we discussed in our latest review, understanding the PL mechanism of Ag NCs is a big challenge for researchers. Although obvious PL intensity enhancement, PLQY increment and longer lifetime performance by doping Ag NCs were observed and the TA method or DFT calculations were applied to explain the experimental results, the universal mechanism of the PL properties is not clear. More studies on the PL mechanism of doped Ag NCs are needed.

(4) Doping improves the properties of Ag NCs, bringing opportunities for practical applications. For bio-application, we need to seriously consider the toxicity of these doped Ag NCs. As we discussed above, the addition of some dopants would lead to an open shell in the kernel, and expose the metals to the solution. This may increase the risk of toxicity. Therefore, the biological properties such as biocompatibility and toxicity of doped Ag NCs should be further explored before their application.

Conflicts of interest

There are no conflicts to declare.

Acknowledgements

J. Y. acknowledges the support from the National Natural Science Foundation of China (Grant No. 51801077). M.-B. L. acknowledges the support from the National Natural Science Foundation of China (Grant No. 92061110), and the Hefei National Laboratory for Physical Sciences at the Microscale (Grant No. KF2020102).

Notes and references

1 R. Jin, C. Zeng, M. Zhou and Y. Chen, *Chem. Rev.*, 2016, **116**, 10346.
2 Q. Yao, T. Chen, X. Yuan and J. Xie, *Acc. Chem. Res.*, 2018, **51**, 1338.
3 T. Udayabhaskararao and T. Pradeep, *J. Phys. Chem. Lett.*, 2013, **4**, 1553.
4 I. Chakraborty and T. Pradeep, *Chem. Rev.*, 2017, **117**, 8208.
5 Y. Du, H. Sheng, D. Astruc and M. Zhu, *Chem. Rev.*, 2020, **120**(2), 526.
6 R. Jin, *Nanoscale*, 2015, **7**, 1549.
7 C. P. Joshi, M. S. Bootharaju and O. M. Bakr, *J. Phys. Chem. Lett.*, 2015, **6**, 3023.
8 A. Ghosh, O. F. Mohammed and O. M. Bakr, *Acc. Chem. Res.*, 2018, **51**, 3094.
9 X. Kang, Y. Li, M. Zhu and R. Jin, *Chem. Soc. Rev.*, 2020, **49**, 6443.
10 T. Kawawaki, Y. Imai, D. Suzuki, S. Kato, I. Kobayashi, T. Suzuki, R. Kaneko, S. Hossain and Y. Negishi, *Chem.–Eur. J.*, 2020, **26**, 16149.
11 X. Kang and M. Zhu, *Chem. Soc. Rev.*, 2019, **48**, 2422.
12 S. Wang, Q. Li, X. Kang and M. Zhu, *Acc. Chem. Res.*, 2018, **51**, 2784.
13 M. S. Bootharaju, C. P. Joshi, M. R. Parida, O. F. Mohammed and O. M. Bakr, *Angew. Chem., Int. Ed.*, 2016, **55**, 922.
14 M. Kim, K. L. D. M. Weerawardene, W. Choi, S. M. Han, J. Paik, Y. Kim, M.-G. Choi, C. M. Aikens and D. Lee, *Chem. Mater.*, 2020, **32**(23), 10216.
15 S. Sharma, K. K. Chakrahari, J.-Y. Saillard and C. W. Liu, *Acc. Chem. Res.*, 2018, **51**, 2475.
16 A. Desireddy, B. E. Conn, J. Guo, B. Yoon, R. N. Barnett, B. M. Monahan, K. Kirschbaum, W. P. Griffith, R. L. Whetten, U. Landman and T. P. Bigioni, *Nature*, 2013, **501**, 399.
17 H. Yang, Y. Wang, H. Huang, L. Gell, L. Lehtovaara, S. Malola, H. Hakkinen and N. Zheng, *Nat. Commun.*, 2013, **4**, 2422.
18 R. S. Dhayal, Y.-R. Lin, J.-H. Liao, Y.-J. Chen, Y.-C. Liu, M.-H. Chiang, S. Kahlal, J.-Y. Saillard and C. W. Liu, *Chem.–Eur. J.*, 2016, **22**, 9943.
19 W.-T. Chang, P.-Y. Lee, J.-H. Liao, K. K. Chakrahari, S. Kahlal, Y.-C. Liu, M.-H. Chiang, J.-Y. Saillard and C. W. Liu, *Angew. Chem., Int. Ed.*, 2017, **56**, 10178.
20 R. S. Dhayal, J.-H. Liao, Y.-C. Liu, M.-H. Chiang, S. Kahlal, J. Y. Saillard and C. W. Liu, *Angew. Chem., Int. Ed.*, 2015, **54**, 3702.
21 C. P. Joshi, M. S. Bootharaju, M. J. Alhilaly and O. M. Bakr, *J. Am. Chem. Soc.*, 2015, **137**, 11578.
22 L. G. AbdulHalim, M. S. Bootharaju, Q. Tang, S. D. Gobbo, R. G. AbdulHalim, M. Eddaoudi, D.-e. Jiang and O. M. Bakr, *J. Am. Chem. Soc.*, 2015, **137**, 11970.
23 J. Yang and R. Jin, *ACS Mater. Lett.*, 2019, **1**, 482.
24 J. Yang and R. Jin, *J. Phys. Chem. C*, 2020, **125**, 2619.
25 J. Yan, H. Su, H. Yang, S. Malola, S. Lin, H. Hakkinen and N. Zheng, *J. Am. Chem. Soc.*, 2015, **137**, 11880.
26 M. S. Bootharaju, C. P. Joshi, M. R. Parida, O. F. Mohammed and O. M. Bakr, *Angew. Chem., Int. Ed.*, 2016, **55**, 922.
27 Y. Li, M. Zhou, S. Jin, L. Xiong, Q. Yuan, W. Du, Y. Pei, S. Wang and M. Zhu, *Chem. Commun.*, 2019, **55**, 6457.
28 M. v. d. Linden, A. J. v. Bunningen, L. Amidani, M. Bransen, H. Elnaggar, P. Glatzel, A. Meijerink and F. M. F. de Groot, *ACS Nano*, 2018, **12**, 12751.
29 X.-Y. Xie, P. Xiao, X. Cao, W.-H. Fang, G. Cui and M. Dolg, *Angew. Chem., Int. Ed.*, 2018, **57**, 9965.
30 Y. Du, Z.-J. Guan, Z.-R. Wen, Y.-M. Lin and Q.-M. Wang, *Chem.–Eur. J.*, 2018, **24**, 16029.
31 B. E. Conn, A. Atnagulov, B. Bhattarai, B. Yoon, U. Landman and T. P. Bigioni, *J. Phys. Chem. C*, 2018, **122**, 13166.

32 A. Baksi, E. K. Schneider, P. Weis, K. R. Krishnadas, D. Ghosh, H. Hahn, T. Pradeep and M. M. Kappes, *J. Phys. Chem. C*, 2019, **123**, 46, 28477.
33 W.-T. Chang, S. Sharma, J.-H. Liao, S. Kahlal, Y.-C. Liu, M.-H. Chiang, J.-Y. Saillard and C. W. Liu, *Chem.–Eur. J.*, 2018, **24**, 14352.
34 Y.-R. Lin, P. V. V. N. Kishore, J.-H. Liao, S. Kahlal, Y.-C. Liu, M.-H. Chiang, J.-Y. Saillard and C. W. Liu, *Nanoscale*, 2018, **10**, 6855.
35 X.-J. Xi, J.-S. Yang, J.-Y. Wang, X.-Y. Dong and S.-Q. Zang, *Nanoscale*, 2018, **10**, 21013.
36 S. Wang, S. n Jin, S. Yang, S. Chen, Y. Song, J. Zhang and M. Zhu, *Sci. Adv.*, 2015, **1**, e1500441.
37 J. Yan, S. Malola, C. Hu, J. Peng, B. Dittrich, B. K. Teo, H. Häkkinen, L. Zheng and N. Zheng, *Nat. Commun.*, 2018, **9**, 3357.
38 J. Yan, H. Su, H. Yang, S. Malola, S. Lin, H. Häkkinen and N. Zheng, *J. Am. Chem. Soc.*, 2015, **137**, 11880.
39 M. S. Bootharaju, S. M. Kozlov, Z. Cao, M. Harb, N. Maity, A. Shkurenko, M. R. Parida, M. N. Hedhili, M. Eddaoudi, O. F. Mohammed, O. M. Bakr, L. Cavallo and J.-M. Basset, *J. Am. Chem. Soc.*, 2017, **139**(3), 1053.
40 X. Kang, L. Xiong, S. Wang, Y. Pei and M. Zhu, *Chem. Commun.*, 2017, **53**, 12564.
41 L. He, J. Yuan, N. Xia, L. Liao, X. Liu, Z. Gan, C. Wang, J. Yang and Z. Wu, *J. Am. Chem. Soc.*, 2018, **140**, 3487.
42 M. S. Bootharaju, S. M. Kozlov, Z. Cao, M. Harb, M. R. Parida, M. N. Hedhili, O. F. Mohammed, O. M. Bakr, L. Cavallo and J.-M. Basset, *Nanoscale*, 2017, **9**, 9529.
43 X. Kang, M. Zhou, S. Wang, S. Jin, G. Sun, M. Zhu and R. Jin, *Chem. Sci.*, 2017, **8**, 2581.
44 M. S. Bootharaju, S. M. Kozlov, Z. Cao, A. Shkurenko, A. M. El-Zohry, O. F. Mohammed, M. Eddaoudi, O. M. Bakr, L. Cavallo and J.-M. Basset, *Chem. Mater.*, 2018, **30**, 2719.
45 X. Kang, L. Huang, W. Liu, L. Xiong, Y. Pei, Z. Sun, S. Wang, S. Wei and M. Zhu, *Chem. Sci.*, 2019, **10**, 8685.
46 X. Lin, C. Liu, K. Sun, R. Wu, X. i. Fu and J. Huang, *Nano Res.*, 2019, **12**, 309.
47 X. Kang, S. Jin, L. Xiong, X. Wei, M. Zhou, C. Qin, Y. Pei, S. Wang and M. Zhu, *Chem. Sci.*, 2020, **11**, 1691.
48 S. Yang, J. Chai, Y. Lv, T. Chen, S. Wang, H. Yu and M. Zhu, *Chem. Commun.*, 2018, **54**, 12077.
49 T.-H. Chiu, J.-H. Liao, F. Gam, I. Chantrenne, S. Kahlal, J.-Y. Saillard and C. W. Liu, *J. Am. Chem. Soc.*, 2019, **141**, 12957.
50 X. Lin, H. Cong, K. Sun, X. Fu, W. Kang, X. Wang, S. Jin, R. Wu, C. Liu and J. Huang, *Nano Res.*, 2020, **13**, 366.
51 S. Kumar Barik, T.-H. Chiu, Y.-C. Liu, M.-H. Chiang, F. Gam, I. Chantrenne, S. Kahlal, J.-Y. Saillard and C. W. Liu, *Nanoscale*, 2019, **11**, 14581.
52 J. Yan, H. Su, H. Yang, C. Hu, S. Malola, S. Lin, B. K. Teo, H. Häkkinen and N. Zheng, *J. Am. Chem. Soc.*, 2016, **138**, 12751.
53 X. Zou, Y. Li, S. Jin, X. Kang, X. Wei, S. Wang, X. Meng and M. Zhu, *J. Phys. Chem. Lett.*, 2020, **11**, 2272.
54 M. S. Bootharaju, H. Chang, G. Deng, S. Malola, W. Baek, H. Häkkinen, N. Zheng and T. Hyeon, *J. Am. Chem. Soc.*, 2019, **141**, 8422.
55 E. Khatun, P. Chakraborty, B. R. Jacob, G. Paramasivam, M. Bodiuzzaman, W. A. Dar and T. Pradeep, *Chem. Mater.*, 2020, **32**, 611.
56 G. Soldan, M. A. Aljuhani, M. S. Bootharaju, L. G. AbdulHalim, M. R. Parida, A.-H. Emwas, O. F. Mohammed and O. M. Bakr, *Angew. Chem., Int. Ed.*, 2016, **55**, 5749.
57 D. Mishra, V. Lobodin, C. Zhang, F. Aldeek, E. Lochner and H. Mattoussi, *Phys. Chem. Chem. Phys.*, 2018, **20**, 12992.
58 X. L. Liu, J. Yuan, C. Yao, J. Chen, L. Li, X. Bao, J. Yang and Z. Wu, *J. Phys. Chem. C*, 2017, **121**, 13848.
59 Y. Liu, X. Chai, X. Cai, M. Chen, R. Jin, W. Ding and Y. Zhu, *Angew. Chem., Int. Ed.*, 2018, **130**, 9923.
60 Z. Qin, S. Sharma, C. Wan, S. Malola, W. Xu, H. Häkkinen and G. Li, *Angew. Chem., Int. Ed.*, 2021, **133**, 983.
61 L. Sun, K. She, H. Sheng, Y. i. Yun, Y. Song, D. Pan, Y. Du, H. Yu, M. Chen and M. Zhu, *J. Catal.*, 2019, **378**, 220.
62 K. Zheng, V. Fung, X. Yuan, D. Jiang and J. Xie, *J. Am. Chem. Soc.*, 2019, **141**, 18977.